*Korean J. Chem. Eng.*, **25**(1), 25-33 (2008)

# Hydraulic-jump behavior of a thin film flowing down an inclined plane under an electrostatic field

**Kwang Seok Kim and Hyo Kim*,†**

Otto H. York Department of Chemical Engineering, New Jersey Institute of Technology, University Heights, Newark, NJ 07102, USA
*Department of Chemical Engineering, University of Seoul, 90 Jeonnong-dong, Dongdaemun-gu, Seoul 130-743, Korea
(*Received 20 February 2007 • accepted 8 May 2007*)

**Abstract**−The hydraulic-jump phenomenon of a thin fluid layer flowing down an inclined plane under an electrostatic field is explored by using a global bifurcation theory. First, the existence of hydraulic-hump wave has been found from heteroclinic trajectories of an associated ordinary differential equation. Then, the jump behavior has been characterized by introducing an intensity function on the variations of Reynolds number and surfave-wave speed. Finally, we have investigated the nonlinear stability of traveling shock waves triggered from a hydraulic jump by integrating the initial-value problem directly. At a given wave speed there exists a certain value of Reynolds number beyond which a time-dependent buckling of the free surface appears. Like the other wave motions such as periodic and pulse-like solitary waves, the hydraulic-jump waves are also found to become more unstable as the electrostatic field is getting stronger.

Key words: Hydraulic Jump, Electrostatic Field, Global Bifurcation Theory, Heteroclinic Trajectory

## INTRODUCTION

The thin film flow has a lot of applications in the engineering fields involving heat and mass transfers due to its transfer efficiency. Hence many researches for the thin film have been performed experimentally and theoretically. As a thin liquid flim flows under the action of gravity down an inclined plane, it is susceptible to surface-wave instabilities. The theoretical study of linear stability in a parallel thin film flow was initiated by Benjamin [1] to identify the stability regimes along the Reynolds number. After this work many authors have analyzed the flow stabilities based on the linear and nonlinear theories - see for examples, Yih [2], Benney [3], Gjevik [4], Lin [5], and Chang [6]. In addition, these kinds of works have been steadily extended by considering the heat transfer into the thin film [7] or by combining the effect of an electrostatic field [8]. They've discussed about the instabilities of the running film flow by gravity with the lubrication theory.

While a thin fluid layer is engaged in the engineering fields we can often see hydraulic-jump phenomena in two limited Reynolds-number regimes. For examples, in a small Reynolds-number flow, that is, when a thin film flows down an inclined plane under gravity and its flow rate is subject to sudden increase or decrease there appears a hydraulic jump on the fluid surface since the flow rate is an increasing function of film height, and in a large Reynolds-number case such as an effective removal of heat emitting from a hot surface of heat exchanger or reactor involving an active exothermic reaction, usually a jet of coolant is spouting from a nozzle to the surface from which the fluid is thinly spreading out and as the flow stream loses its inertial force away from the impinging area we see a hydraulic jump occurring in the downstream. When the surface wave triggered from the jump is traveling downward it is usually called a shock wave whose amplitude depends on its velocity. This kind of finite-amplitude traveling wave has been characterized through the nonlinear analysis of its model evolution equation. The hydraulic jump acts as an another unstable factor to the flow system and hence its analysis is desirable to understand its stability. For the Reynolds number of order one Pumir et al. [9] examined the hydraulic-jump phenomenon briefly on their way to seeking solitary waves running down an inclined plane. In a moving frame steady at a certain speed they took on heteroclinic trajectories which connect the Nusselt base state to the thicker layer for the description of hydraulic jump from the point of view of dynamical system theory. They also observed a time-dependent buckling of the free surface at a specific value of Reynolds number. Prokopiou et al. [10] described the amplitude-velocity relationships of shocks during their analysis of long waves on inclined films at a high Reynolds number by employing a second-order integral boundary-layer approximation.

The application of an electrostatic field to the thin film flow has been practically proposed to answer the feasibility of new design concepts for a space radiator called Electrostatic Liquid Film Radiator (ELFR). The first kind of ELFR concept was the plane-flow radiator [8] as a local approximation for a radiator with a small radial curvature. The second one was the rotating conical or tapered-disk radiator to optimize the effective driving force and hydrostatic pressure for film stability and weight minimization [11]. In addition, for a small Reynolds-number case Kim [12] considered the electrified thin-film plane flow in the view point of the nonlinear stability by using a two-dimensional wave evolution and its characterized pulse-like solitary waves. It was found the charged electrostatic field always rendered the flow system more unstable in proportional to applied amount of electric strength. Other applications of electric field can be found recently in the polymer film processing to get a desirable structure formation and pattern transfer. Schäffer et al. [13] showed

†To whom correspondence should be addressed.
E-mail: hkim@uos.ac.kr

a simple electrostatic technique to create and replicate lateral structures in polymer films on a submicrometer length scale. In addition to this, in 2001 Schäffer et al. [14] exploited the wave pattern caused by an electrohydrodynamic instability to get non-equilibrium pattern formation in quasi-two-dimensional systems. Lin et al. [15] reported a systematic characterization of structure formation at the interface of liquid/liquid bilayers in an electric field. These researches have used the surface deformation effect made by the electrohydrodynamic instability.

Considering the application of an electric field to the thin film flow we are certainly inquisitive about the wave instability caused by an abruptly changed film thickness because the initially dislocated fluid layer due to the variation of flow rate will be more disturbed by the applied electric field. That is, unstable waves caused from the hydraulic jump will be getting amplified downstream and the charged-foil system might be sparkover and breakdown as the waves are drastically growing up to the brim of the charged foil. Hence, in this paper, first we explore the existence of shock waves by using an orbit heteroclinic to a fixed point in a linearized third-order ordinary differential equation obtained in a steady moving frame of the evolution equation used previously by Kim [12]. Then we examine the nonlinear behavior of traveling shock waves obtained by solving the initial-value problem directly at given values of film-height difference between up-and downstream and electric field intensity. Here it has to be noted for an initial condition the upstream thickness is always taken thicker than the downstream because if the downstream would be thicker its surface-wave speed in the streamwise direction is faster than the upstream's one (since the flow rate depends proportionally to the film height in our flow system) and therefore the initially set-up steep face is stretching out and making no traveling shock waves.

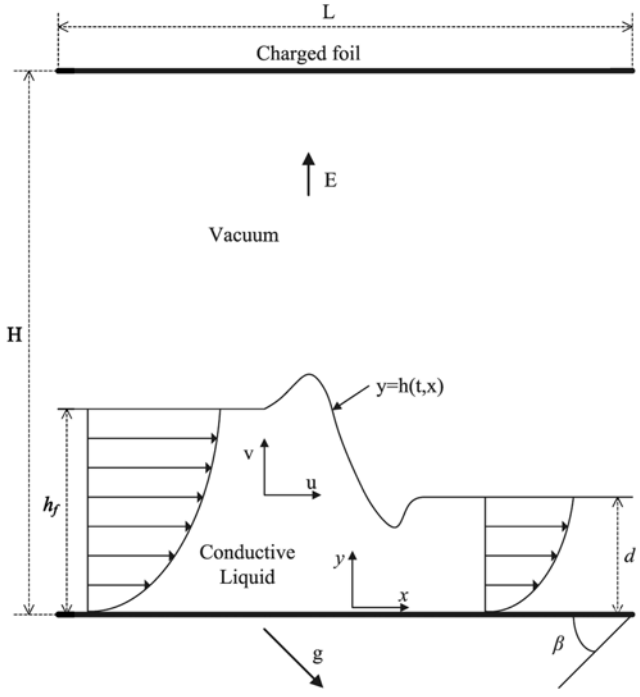


**Fig. 1. Hydraulic-jump flow system under a uniform electrostatic field.**

## EVOLUTION EQUATION FOR A LOCAL FILM THICKNESS

The liquid layer is assumed an isothermally incompressible and dielectric Newtonian viscous fluid whose density and viscosity are taken $\rho$ and $\mu$, respectively. It runs down an inclined plane under the action of gravity g. Two-dimensional case will be only considered here and the plane is assumed to make an angle $\beta$ with the horizontal, and we choose the coordinate system such that the x axis is parallel to the plane while the y axis is perpendicular to it (Fig. 1). Above the liquid layer there is a vacuum whose vapor pressure is neglected. Within the vacuum region at a distance H from the plane of length L locates a charged foil which has the same dimension as the plane as shown in Fig. 1. The dielectric constants of the vacuum and the liquid layer are $\varepsilon_0$ and $\varepsilon_f$, respectively, and the ratio is defined as $\varepsilon=\varepsilon_f/\varepsilon_0$. An electrostatic field from the charged foil with an electric potential F will interact with the liquid flow through the induced pulling-over force. Suppose that d is defined as the characteristic thickness of the primary film flow before the hydraulic jump occurs and employed as a scale factor for y-direction quantities, then the parameter $\xi$=d/L will be very small if the film is thin, i.e., thin relative to the expected length scale L which is used for the nondimensionalization of the variables in the horizontal. For convenience's sake the center of the plane is set x=0 and the fluid surface is taken flat as $x\rightarrow\pm\infty$. We have set the front upstream film thickness as $h_f$ to denote the upheaved layer while the downstream is kept at one. In this study, the Reynolds number Re is defined as

$$\mathrm{Re}=\frac{\rho U_0 d}{\mu}, \tag{1}$$

and its order keeps unity. $U_0$ is a characteristic velocity, which is based on the maximum velocity of the basic plane flow. To measure the relative importances of surface tension $\sigma$ of the liquid and gravity to the fluid inertial force, respectively, we define the capillary number Ca and the Froude number Fr such as

$$\mathrm{Ca}=\frac{2\mu U_0}{\sigma}, \tag{2}$$

and

$$\mathrm{Fr}^2=\frac{U_0^2}{gd}. \tag{3}$$

The basic knowledge about this 2-dimensional flow enables us to combine Eq. (1) and Eq. (3) to get

$$\frac{\mathrm{Re}}{\mathrm{Fr}^2}\sin\beta=2. \tag{4}$$

And the last dimensionless group K to consider the effect of an applied electrostatic field is set by

$$\mathrm{K}=\frac{\varepsilon_0 dF^2}{16\pi\mu U_0}. \tag{5}$$

The derivation of the equation ruling the evolution of film thickness h(x, t) and its linear stability analysis have been already performed with a perfect conductor, i.e., $\varepsilon\rightarrow\infty$ [12,16]. Hence, we will use the same evolution equation of the film surface obtained by Kim [12] except that the effect of a dimensionless dielectric constant is

included here, i.e.,

$$h_t + 2h^2h_x + \xi\frac{\partial}{\partial x}\left(\frac{8}{15}\mathrm{Re}h^6h_x - \frac{2}{3}\mathrm{B}h^3h_x + \frac{2}{3}\frac{\xi^2}{\mathrm{Ca}}h^3h_{xxx}\right) - \frac{4}{3}\xi\mathrm{K}\left(\frac{1}{\varepsilon}-1\right)\frac{\partial}{\partial x}\left(\frac{H^2h^3h_x}{\left(H+\left(\frac{1}{\varepsilon}-1\right)h\right)^3}\right) = 0, \quad (6)$$

where B is a cotangent of $\beta$, and the subscript means a partial derivatives with respect to the variables in it. From now on we will employ Eq. (6) to find out the hydraulic-jump shock waves and carry out its nonlinear dynamic analysis.

## HYDRAULIC JUMP IN A MOVING FRAME

As previously mentioned, solitary waves in a falling film with or without an electrostatic field have two types: a pulse-like wave or a hydraulic-jump shock wave. The extended research for the pulse-like solitary wave has already been done under the influence of an electrostatic field [12]. In this section we are searching for a special solution of Eq. (6) generating hydraulic-jump shock waves. Reminding that hydraulic-jump wave travels without change of its shape, thus if we let the reference coordinates move at the same velocity of the running hydraulic-jump wave, then the wave looks like a stationary wave. Mathematically, this moving coordinates can be expressed as z=x−vt and then the time-dependent term in the partial differential equation is dropped out and Eq. (6) turns into a third-order ordinary differential equation. Here, v is the velocity of the hydraulic-jump wave. By using chain rule in the applications of z into Eq. (6) and then keeping the Nusselt flat film conditions far away, that is, $h_z$ and $h_{zz}$ going to zero as $z\to\pm\infty$, we obtain the following equation after integrating Eq. (6) once with respect to z from $-\infty$ to $\infty$,

$$-\frac{3}{2}vh + h^3 + \frac{4}{5}\left[\mathrm{Re}h^3 - \frac{5}{4}\mathrm{B} - \frac{5}{2}\mathrm{K}\left(\frac{1}{\varepsilon}-1\right)\frac{H^2}{\left(H+\left(\frac{1}{\varepsilon}-1\right)h\right)^3}\right]h^3h' + \frac{1}{\mathrm{Ca}}h^3h''' = 1-\frac{3}{2}v. \quad (7)$$

Here the prime denotes the derivative with respect to z and we let h(z)=1 as $z\to\infty$.

Unlike a pulse-like solitary wave, the upstream film thickness $h_f$ is different from the downstream and thus it has to be determined with v. To do this, Eq. (7) has been mapped into 3 dimensional phase space defined as ($U_1$, $U_2$, $U_3$) where $U_1$=h, $U_2$=h′ and $U_3$=h″. Hence Eq. (7) can be transformed into

$$\begin{aligned} U_1' &= U_2, \\ U_2' &= U_3, \\ U_3' &= \mathrm{Ca}\left[\frac{1-U_1}{U_1^3}\left(1+U_1+U_1^2-\frac{3}{2}v\right) - \frac{4}{5}\left(\mathrm{Re}U_1^3 - \frac{5}{4}\mathrm{B} - \frac{5}{2}\left(\frac{1}{\varepsilon}-1\right)\frac{KH^2}{\left(H+\left(\frac{1}{\varepsilon}-1\right)U_1\right)^3}\right)U_2\right]. \end{aligned} \quad (8)$$

It is very hard to find out the phase trajectories of Eq. (8) analytically due to its nonlinearity. Therefore to seek for the phase portrait qualitatively, we have to figure out the phase portrait of the corresponding linearized system about the critical points. First, the critical points of Eq. (8) are found as

$$U_2 = U_3 = 0,\ (U_1-1)\left(U_1^2+U_1+1-\frac{3}{2}v\right) = 0. \quad (9)$$

We find there are two kinds of critical points, i.e., ($U_1$, $U_2$, $U_3$)=(1, 0, 0) or ($U_1$, $U_2$, $U_3$)=($h_f$, 0, 0). The linearized system about the first fixed point ($U_1$, $U_2$, $U_3$)=(1, 0, 0) had already been used for the analysis of pulse-like solitary wave whose phase is homoclinic by Kim [12]. In the second fixed point, the $h_f$ is a positive root of

$$h_f^2 + h_f + 1 - \frac{3}{2}v = 0, \quad (10)$$

and due to this value of $h_f$ the linearized Eq. (8) around the second critical point will show the hydraulic-jump behavior of the system. That is, near the fixed point ($h_f$, 0, 0) the linearized system of Eq. (8) can be expressed as

$$\vec{\mathbf{U}}' = [\mathrm{A}]\vec{\mathbf{U}}, \quad (11)$$

where

$$\vec{\mathbf{U}} = (U_1, U_2, U_3)^T,$$

$$[\mathrm{A}] = \begin{pmatrix} 0 & 1 & 0 \\ 0 & 0 & 1 \\ \phi_1 & \phi_2 & 0 \end{pmatrix},$$

$$\phi_1 = \frac{3}{2}\frac{\mathrm{Ca}}{h_f^3}(v-2h_f^2),$$

and

$$\phi_2 = -\frac{4}{5}\mathrm{Ca}\left[\mathrm{Re}h_f^3 - \frac{5}{4}\mathrm{B} - \frac{5}{2}\frac{\mathrm{K}\left(\frac{1}{\varepsilon}-1\right)H^2}{\left(H+\left(\frac{1}{\varepsilon}-1\right)h_f\right)^3}\right]. \quad (12)$$

T means the transpose of a vector. Assume $\lambda$ is an eigenvalue of the Jacobian matrix [A], then the characteristic equation to determine $\lambda$ is found as

$$\lambda^3 - \phi_2\lambda - \phi_1 = 0. \quad (13)$$

To ensure the linearized Eq. (11) shows a hydraulic jump, $\phi_1$ in Eq. (13) always has to be negative because the eigenvalue system should have one-dimensional stable and two-dimensional unstable manifolds contrary to the case of the pulse-like solitary wave [17]. If we set $\lambda_1=2\rho$ and $\lambda_{2,3}=-\rho\pm i\omega$ with real $\rho$ and $\omega$, then the $\lambda$'s are certainly satisfied with Eq. (13), and with $\rho<0$ it is clear Eq. (11) really has one-dimensional stable and two-dimensional unstable manifolds. For $\rho<0$, $h_f$ has to be greater than $\sqrt{v/2}$ which can be derived from $\phi_1=\lambda_1\lambda_2\lambda_3=2\rho(\rho^2+\omega^2)$. In general, the two-dimensional manifold will be connected to a two-dimensional stable manifold created by the other critical point ($U_1$, $U_2$, $U_3$)=(1, 0, 0). The trajectory joining these two different critical points is called heteroclinic [17]. The heteroclinic orbit is a solution describing a hydraulic-jump shock wave with a height $h_f$ upstream and h=1 downstream. Here we will consider $h_f>1$ (v>2) as we have already mentioned in the section of Introduction.

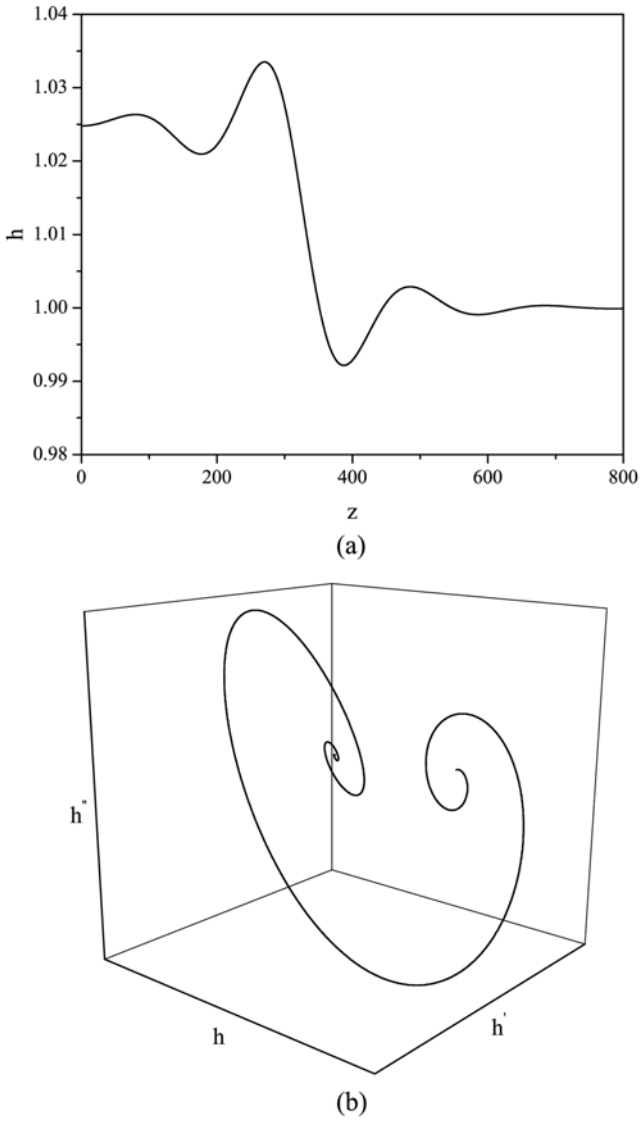


**Fig. 2. (a) A hydraulic jump found with Re=7.239733328, v=2.05, Ca=1/3,000, H=10, $\varepsilon$=2, B=5 and K=10, and (b) its heteroclinic orbit in three-dimensional phase space.**

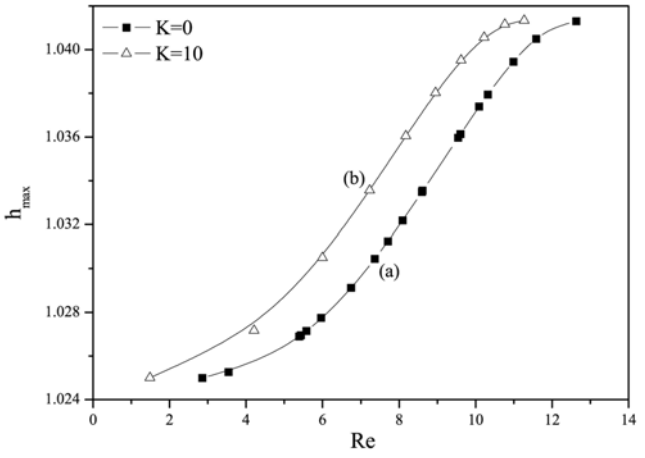


**Fig. 3. The existence of a hydraulic-jump wave is shown in a Re–$h_{max}$ plane with K=0 and K=10. The points (a) and (b) are selected to show in Fig. 4 how much an electrostatic field affects the shape and stability of a hydraulic jump as an example where (a) for a free-charged case (K=0) and (b) for a charged case (K=10).**

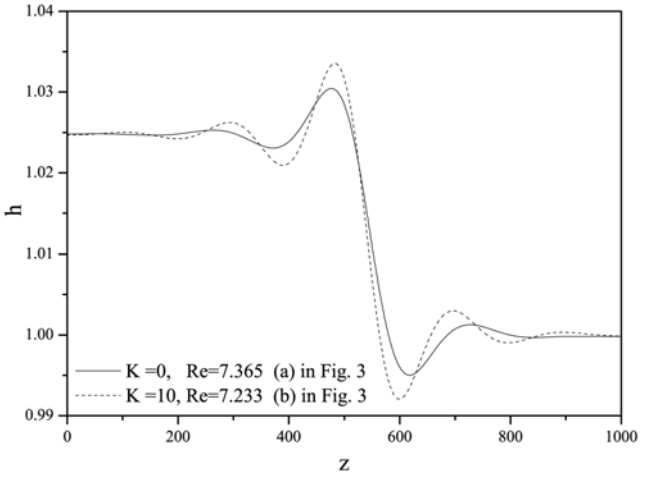


**Fig. 4. The hydraulic-jump shock waves are plotted at points (a) and (b) in Fig. 3.**

Fig. 2 shows the calculation result of a hydraulic jump in a moving frame by solving Eq. (8). The solution has been chased by a shooting scheme starting from ($h_f$, 0, 0) and adjusting Re until the trajectory satisfies the boundary condition ($U_1$, $U_2$, $U_3$)=(1, 0, 0) at some large z. The purpose of this calculation is to seek the existence of a hydraulic-jump wave and how the applied electrostatic field affects it. Thus, keeping v=2.05, Ca=1/3,000, H=10, $\varepsilon$=2, B=5, and K=10 fixed, we have discovered a hydraulic-jump shock wave at Re=7.239733328 as in Fig. 2(a). Fig. 2(b) shows its 3-dimensional phase-portrait orbit heteroclinic to its fixed points: ($h_f$, 0, 0) located right is a source while the left (1, 0, 0) is a sink. Now in the same manner but with no electrostatic field, i.e., K=0, we have reached the same profile of a hydraulic-jump wave at a higher value of Reynolds number, i.e., Re=8.609423022. From this calculation we have known the applied electric strength reduces the onset Reynolds number of the hydraulic-jump wave which has the same wave speed as in the free-charged case, that is, the electrostatic field acts as an instability on the nonlinear dynamics of a hydraulic-jump shock wave.

In order to extend the instability problem in a comprehensive manner, we have traced more hydraulic-jump waves by varying the Reynolds number and finally plotted the results in a $h_{max}$ vs. Re domain as in Fig. 3. Fig. 3 supports our expectation of the hydraulic-jump instability, that is, the higher Re at both K=0 and K=10, the more unstable, and at a fixed Re the flow with K=10 (existence of electrostatic force) also shows more instability than with K=0 (free charge). The points (a) and (b) in Fig. 3 are selected to show in Fig. 4 how much an electrostatic field affects the shape and stability of a hydraulic jump as an example where (a) for a free-charged case (K=0) and (b) for a charged case (K=10). Here we have noted the searching scheme for the heteroclinic orbit is tricky because it is very sensitive to the parameters. Hence we have adopted slightly different Re values (at which it is available to construct the heteroclinic orbits) to compare the shapes of a hydraulic-jump shock

wave as in Fig. 3.

## INTENSITY OF A HYDRAULIC-JUMP WAVE

In the previous section the existence condition and the shape of a hydraulic-jump wave have been identified by finding out a heteroclinic trajectory. Now in this section we will discuss about the behavior of hydraulic-jump shock wave more analytically. To do this we first integrate Eq. (7) divided by $h^3$ once with z from $-\infty$ to $\infty$, and the result is

$$\int_{-\infty}^{+\infty}\frac{h-1}{h^3}\left(h^2+h+1-\frac{3}{2}v\right)dz + \frac{4}{5}\left[\frac{1}{4}Reh^4-\frac{5}{4}Bh-\frac{5K}{2H}\left(\frac{1}{\varepsilon}-1\right)h\right]_{h_f}^{1}=0. \quad (14)$$

Here $H+(1/\varepsilon-1)h$ approximates to H since $H>>h$. By letting $\Delta h=h_f-1$, finally Eq. (14) is transformed into

$$\mathbf{I}=\int_{-\infty}^{+\infty}\frac{h-1}{h^3}\left(h^2+h+1-\frac{3}{2}v\right)dz = \frac{1}{5}Re[4(\Delta h)+6(\Delta h)^2+4(\Delta h)^3+(\Delta h)^4] + (\Delta h)\left(-\frac{2K}{H}\left(\frac{1}{\varepsilon}-1\right)-B\right). \quad (15)$$

We have set the integral form by **I** and we will call it an intensity of the hydraulic jump because it represents another form of surface-wave momentum. Since $(1/\varepsilon-1)<0$, the only factor that makes **I** negative is B. With larger $\beta$ (or smaller B), the value of **I** grows bigger, and finally with $\beta=\pi/2$ (i.e., vertically falling film), i.e., there is no gravity component contributing to the flow stability, the hydraulic-jump wave will reach to its maximum value of intensity if the other parameters are fixed. From this fact, we know again that B is acting as a stability while Re and K terms make the flow unstable. The greater **I** the flow retains, the more unstable shock waves will show up. Another aspect of this intensity is that it is a linear function of Re with its slope determined only by $\Delta h$ and its intercept by an applied electrostatic field strength and B.

To demonstrate the shape of the hydraulic-jump shock wave according to **I** value, we need to calculate several equi-intensity lines in the domain of Re versus v as shown in Fig. 5. For this purpose, first we have to replace $\Delta h$ terms in Eq. (15) with v by using the relation $\Delta h=(\sqrt{6v-3}-3)/2$. Finally, we can get the following result

$$Re=\frac{5\mathbf{I}+\frac{5}{2}(\sqrt{6v-3}-3)\left[\frac{2K}{H}(1/\varepsilon-1)+B\right]}{-\frac{3}{2}+\frac{1}{2}\sqrt{6v-3}(1-3v)+\frac{9}{4}v^2}. \quad (16)$$

Plugging several **I** values into Eq. (16) we obtained the equi-intensity map as in Fig. 5 by keeping K=10, H=10, $\varepsilon$=2 and B=5. When **I**=0, Eq. (16) is simplified to

$$Re_{I=0}=\frac{10\frac{K}{H}(1/\varepsilon-1)+B}{1-\frac{3}{4}v+\frac{3}{4}v\sqrt{6v-3}}. \quad (17)$$

If we let v=2 in the above equation, then the Reynolds number becomes

$$Re_{v=2}=\frac{5}{4}\left[\frac{K}{H}(1/\varepsilon-1)+B\right] \quad (18)$$

which is a cut-off Reynolds number acquired form the linear stability analysis of a plane flow without a surface tension effect [12]. From the integrand of Eq. (15) we can predict the shape of a hydraulic jump to make **I**=0. That is, as the upstream and downstream are flat and the face of shock wave is a cliff such as a step function, naturally the integrand goes to zero. We can't achieve this kind of hydraulic-jump wave in a real physical system.

Now by selecting four different points of (a), (b), (c) and (d) to the various **I** values in Fig. 5, we have illustrated the corresponding hydraulic-jump waves in Fig. 6. At first sight it is evident that a hydraulic-jump wave with a higher value of intensity develops into a bigger and steeper hump on the upstream and a deeper well on the downstream around the jump location in comparison with a smaller.

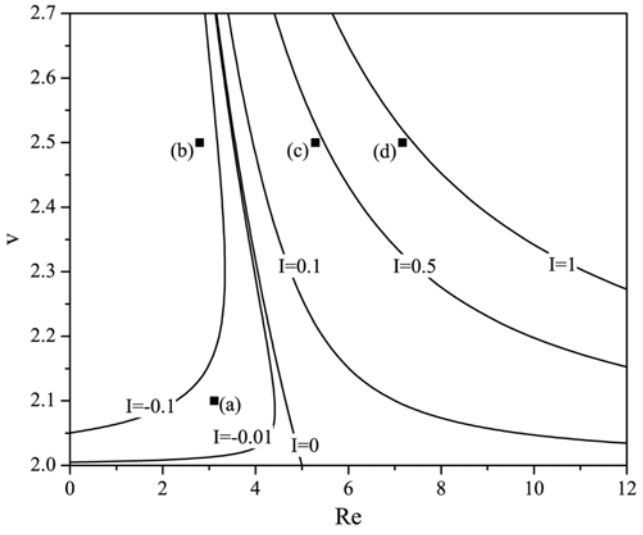


**Fig. 5. Equi-intensity lines in Re–v plane which are calculated from Eq. (16) with K=10, H=10, $\varepsilon$=2 and B=5.**

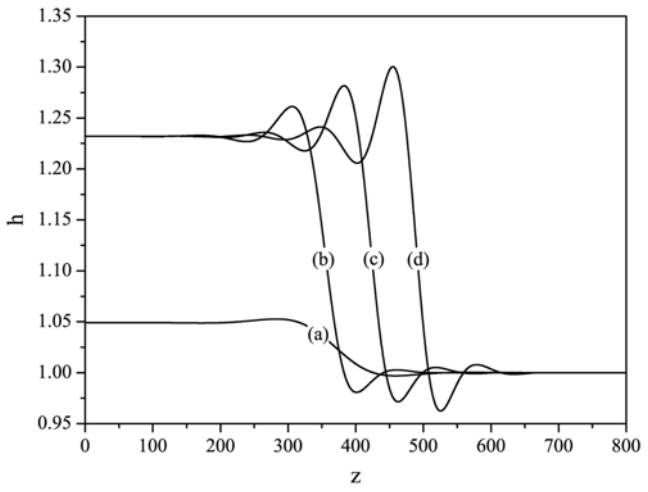


**Fig. 6. The hydraulic-jump waves at the points of (a), (b), (c) and (d) in Fig. 5 to compare their shapes to the various intensities.**

In addition to this fact, we have to mention another trend of a hydraulic-jump wave in the negative domain of **I**. To guarantee the integration result in Eq. (15) to be negative, the shock has to be flat without any deformation while the steep face is spreading out (the bigger negative value means the more spreading out of the shock face). It can be easily proved when we perform the integration of Eq. (15) after substituting $h=h_f+((1-h_f)/(z_2-z_1))(z-z_1)$, where the upstream constant film thickness is $h_f$ at $z=z_1$ and the film height of downstream is set as one at $z=z_2$ ($z_2>z_1$). Seeing the wave shape of (a) in Fig. 6 we can understand the wave face is stretched and the film heights in the up-and downstreams are flat in the negative **I**.

For an analytical approach to a limit case, we have set $v\rightarrow 2$, i.e. $\Delta h\rightarrow 0$ so that $\Delta h^2$, $\Delta h^3$ and $\Delta h^4$ can be neglected. Then from Eq. (15) we get the result

$$\mathrm{Re}=\frac{5}{4}\frac{\mathbf{I}}{\Delta h}+\mathrm{Re}_{v=2}. \tag{19}$$

Thus we can get the differentiation result:

$$\frac{d\mathrm{Re}}{d(\Delta h)}=-\frac{5}{4}\frac{\mathbf{I}}{\Delta h^2}. \tag{20}$$

And reminding that $\Delta h\sim\sqrt{v}$, hence $d(\Delta h)\sim v^{-1/2}dv$. Therefore Eq. (20) reduces to

$$\frac{d\mathrm{Re}}{dv}\sim-\frac{\mathbf{I}}{v^{3/2}}, \tag{21}$$

From this result we can anticipate the slope of dRe/dv around v=2 which is directly determined by the sign of **I**. We can check Fig. 6 supports this approximation very well around v=2.

## NUMERICAL RESULTS

Up to now, we have sought special solutions of Eq. (6) by using a steady moving frame which offered an easy analytical way to seek and characterize hydraulic-jump shock waves in an ordinary differential system. However, the real evolution is time-dependent and thus it is necessary to confirm the formation of hydraulic-jump shock waves that will dominate all subsequent interfacial dynamics. In this section, time-dependent problem will be treated by directly integrating Eq. (6). To solve the initial-value problem we first have to consider the computational domain. Due to the different film heights on the layer, here we cannot hire the periodic domain as in the pulse-like solitary waves [12]. And it is also impossible to extend the domain to a sufficiently large space to include all of the wave transitions because a tremendous amount of time will be required for the computation. Therefore, to shoot this kind of problem and secure the laterally unbounded flow region, we have let the x-coordinate move ahead as the wave propagates. If the speed of the coordinate is properly tuned up, we can make the surface-wave developments standstill.

To integrate Eq. (6), we have employed the Crank-Nicolson scheme using the centered difference in space and forward difference in time, and the spatial stepsize has been halved till the solutions converge. The first and the second derivatives of the surface kept to be zero at both ends of the computational domain, which denotes the flat boundary conditions. And we have the initial shock wave consisting of the flat upstream (=$h_f$>1) and downstream (h=1) with a cosine-

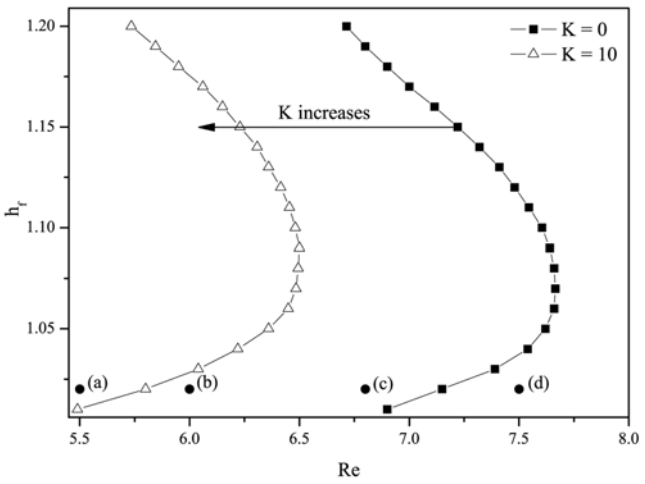


**Fig. 7. $h_f$ versus Re for delineating the appearance of hydraulic-jump and time-dependent buckling waves. In the left region of each line the hydraulic-jump shock waves always appear while in the right region there are time-dependent buckling waves. The points (a), (b), (c) and (d) are selected to show the phenomena in Fig. 8.**

descending face conjoining those two streams. An arbitrary selection of the face shape doesn't affect finally developed profile of an hydraulic-jump shock wave. In the integrations, we have $\xi$=0.02, Ca=1/3,000, B=5, H=10 and $\varepsilon$=2 fixed while choosing K=0 or K=10.

Prior to illustrating, the initial wave is evolving to a hydraulic-jump shock wave in the t−x domain, through a lot of computations with various $h_f$ and Re values we have built up a diagram dividing two regions in a $h_f$–Re, that is, one stands for the appearance of hydraulic-jump shock waves and the other for the time-dependent buckling waves which make the flow unstable with many dimples on the upstream in the long run.

The results of the numerical calculations are summarized in Fig. 7, showing two curves in a $h_f$−Re plane. Each curve represents the borderline between the existence of hydraulic-jump and time-dependent buckling waves. The right one is calculated in the absence of an electrostatic field (K=0) while the left one is in the presence of an electrostatic field (K=10). We have found that within the left region of each curve there always exists a hydraulic-jump wave and beyond it to the right there appears a time-dependent buckling wave. Note that the curve moves left as an electrostatic field gets stronger, which means the area where hydraulic-jump wave can exist gets smaller and smaller. The applied electrostatic field renders the hydraulic-jump wave more unstable to a buckling. These facts are exhibited in Fig. 8 by choosing the points of (a), (b), (c) and (d) in Fig. 7. Here we have selected Re as 5.5, 6.0, 6.8 and 7.5 but kept $h_f$ as 1.02.

In Fig. 8, the lowest surface wave is an initial condition for the integration of Eq. (6). With the time interval between adjacent lines, i.e., $\Delta t$=50, the shape of the surface wave is recorded and piled up. As expected in Fig. 7, once the initial surface waves in (a) and (c) have reached the hydraulic-jump shock waves they propagate downstreams holding on their shapes without any dissipation, on the other hand in (b) and (d) the time-dependent ripples and bucklings are

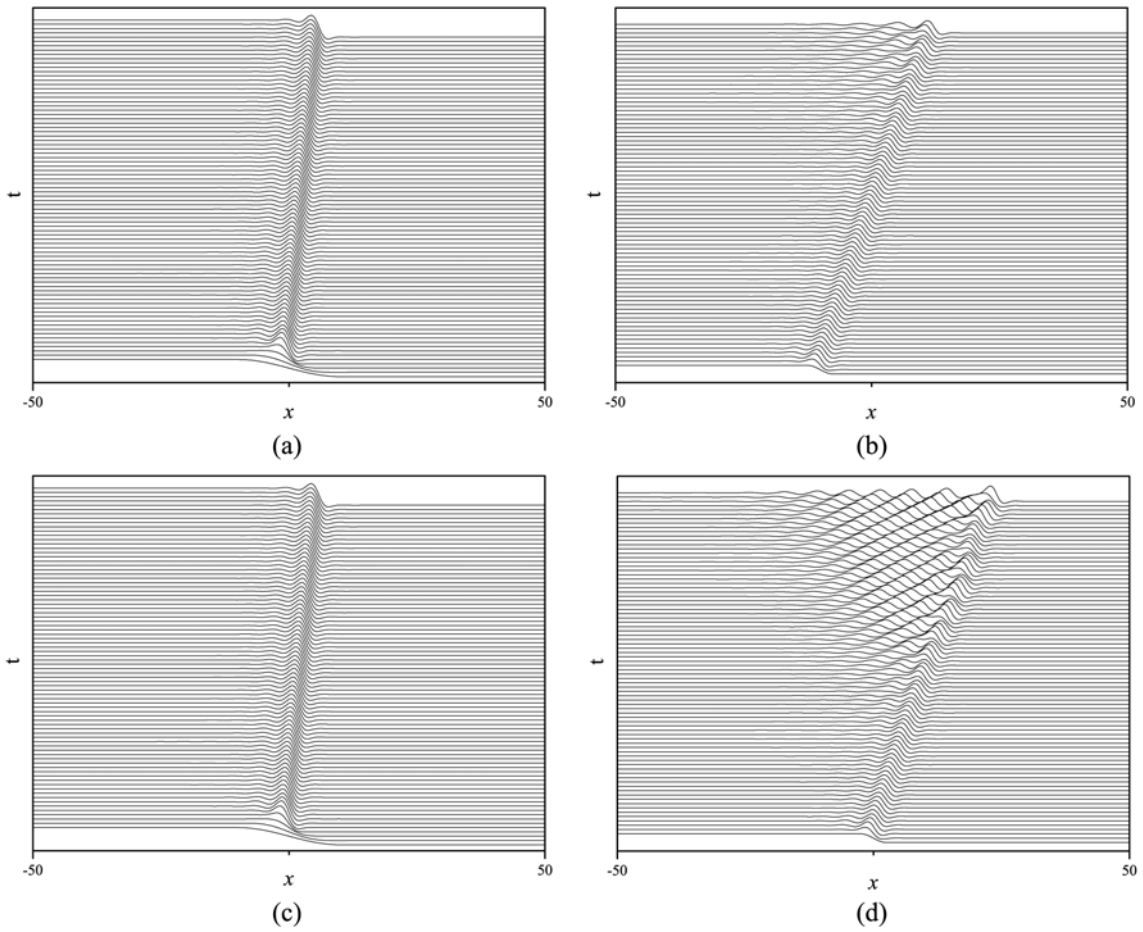


**Fig. 8. The examples of the numerical evolutions of Eq. (6) with $h_f$=1.02: (a) Re=5.5, K=10, (b) Re=6.0, K=10, (c) Re=6.8, K=0, and (d) Re=7.5, K=0.**

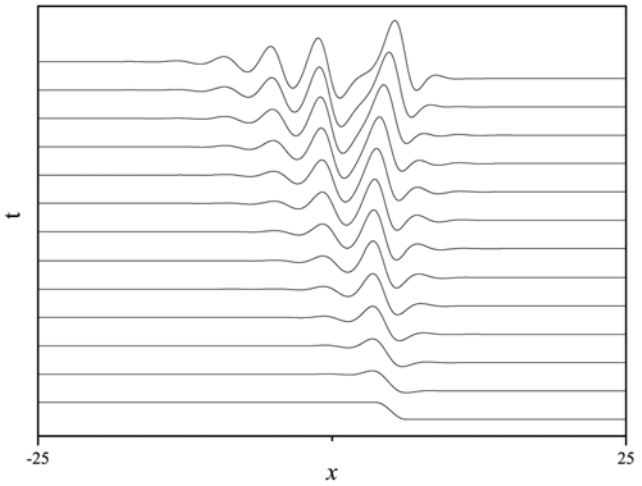


**Fig. 9. The evolution of a shock wave instability when an extremely high electrostatic field such as K=50 has been applied.**

detected. The applied electrostatic field certainly makes the Reynolds number retaining the hydraulic-jump wave smaller and the flow more unstable. Here both speeds of actual wave and x-coordinate are around 2.04.

Now we will focus on the effect of a strong electrostatic field on the film evolution. To do this, the integration was performed again with the much strongly applied electrostatic field, K=50 but rather smaller Reynolds number Re=3. The rapid growth of the surface wave makes the shock face steeper and generates big time-dependent bucklings on the upstream site as in Fig. 9. As the shock wave gets higher, the local phase speed of the wave is accelerating. Therefore, the traveling speed of the shock crest on the upstream is greater than that of the downstream. Accordingly the shock wave will soon break and show a catastrophic behavior. In Fig. 9 the computation work with the Crank-Nicolson method is terminated at t=120. To magnify the graph in Fig. 9, we have the range of x coordinate in Fig. 9 shorten to a half of that in Fig. 8.

Finally, we have charcterized the hydraulic-jump shock wave calculated from our numerical study as the relationship between its maximum height and the Reynolds number (see Fig. 10). The black symbols denote the results without an electrostatic field and empty ones are at K=10. Letting the upstream thickness take up three values such as 1.06, 1.1 and 1.16, the maximum heights of hydraulic-jump shock waves are computed by changing the Reynolds number from one to four, respectively. The results are plotted on the domain of $h_{max}-h_f$ versus Re, where we have adopted $h_{max}-h_f$ instead of $h_{max}$ because we have to focus only on how much Reynolds number and upstream thickness disturb the surface wave dynamically comapred with the upstream thickness. Qualitatively, in the small

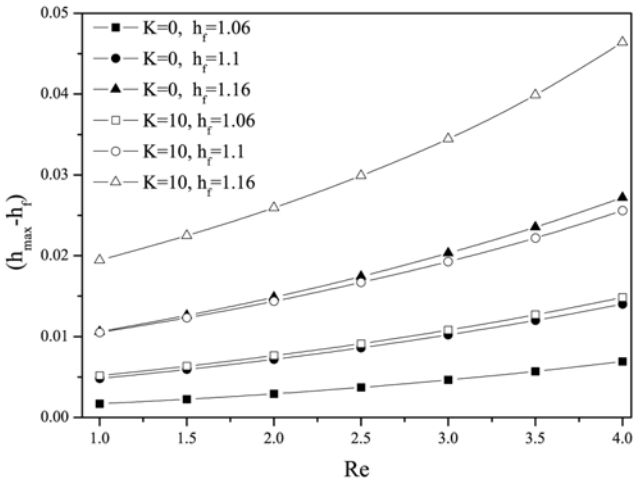


**Fig. 10. ($h_{max}$−$h_f$) versus Re for $h_f$=1.06, 1.1 and 1.16 according to K=0 and K=10, respectively.**

Reynolds number region from around 1 to 2.5, $h_{max}$−$h_f$ grows linearly. But over some Reynolds number, i.e. beyond about 2.5, the growing rates of $h_{max}$−$h_f$ with increasing Re become faster and faster. Also the increasing rate is affected by both $h_f$ and K.

## CONCLUSIONS

First, the hydraulic-jump behavior of a thin fluid layer flowing down an inclined plane under an electrostatic field is investigated by employing a global bifurcation theory. The existence of hydraulic-hump wave has been found from heteroclinic trajectories of an linearized ordinary differential Eq. (11) which is transformed from the nonlinear surface-wave evolution mechanism defined by Eq. (6). That is, introducing a steady moving frame into Eq. (6) we have obtained the third-order ordinary differential Eq. (11), and then the existence of hydraulic-jump wave and its orbit heteroclinic to the fixed points in the three dimensional phase space has been searched by the structural stability theory. Next, the intensity **I** of a hydraulic-jump shock wave has been newly defined to see the relative significance of the parameters involing the hydraulic-jump wave gestation. And some special region of the equi-intensity in a v−Re domain has been turned out to be associated with the critical Reynolds number in the linear stability theory. An applied electrostatic field makes the hydraulic-jump shock wave have a steeper face and higher amplitude. Finally, the direct integration of Eq. (6) has been carried out to find the existence of a time-dependent hydraulic-jump wave, and to confirm if the characteristics found in a moving frame match with the results of the numerical simulations. In this numerical study, the $h_f$−Re region has been divided into two parts: one is for the appearance of hydraulic-jump shock waves, and the other for coming-out of the time-dependent buckling waves. And an electrostatic field shrinks the area of the former region and when even higher electrostatic field is applied we have obtained a catastrophic breaking wave, in other words, it acts as an instability factor to the hydraulic-jump shock wave. Considering all of these facts calculated from the nonlinear dynamics, the characteristics of hydraulic-jump shock waves defined in the evolution Eq. (6) have shown that the increasing upstream film thickness as well as a stronger electrostatic-field application makes the hydraulic-jump shock wave running down an inclined plane vulnerable to instability.

## ACKNOWLEDGMENT

This study was performed by the support from the University of Seoul in 2006, and the authors gratefully acknowledge it.

## NOMENCLATURE

B : cot$\beta$
Ca : capillary number
d : characteristic film thickness
F : electrostatic potential of foil
Fr : Froude number
g : gravity
H : dimensionless distance from plane to charged foil
h : local film thickness
**I** : relative intensity of hydraulic jump
K : dimensionless electric force constant
L : characteristic length scale parallel to plane
Re : Reynolds number
t : dimensionless time
$U_0$ : characteristic velocity parallel to plane
$U_1$ : h
$U_2$ : h′
$U_3$ : h″
$h_f$ : dimensionless thickness of the upstream
v : dimensionless wave velocity
x : dimensionless distance coordinate parallel to plane
z : x − vt

### Greek Letters

$\beta$ : inclination angle of plane with the horizontal
$\Delta h$ : $h_f$ − 1
$\varepsilon$ : $\varepsilon_f/\varepsilon_0$
$\varepsilon_0$ : dielectric constant of air
$\varepsilon_f$ : dielectric constant of liquid
$\mu$ : viscosity of liquid
$\xi$ : d/L
$\rho$ : mass density of liquid
$\sigma$ : surface tension of liquid

### Superscripts

′ : derivative with z
t : transpose of a vector

### Subscripts

max : maximum value
t : partial derivative with t
x : partial derivative with x

## REFERENCES

1. T. B. Benjamin, *J. Fluid Mech*., **2**, 554 (1957).
2. C.-S. Yih, *Phys. Fluids*, **5**, 321 (1963).
3. D. J. Benney, *J. Math. & Phys*., **45**, 150 (1966).

4. B. Gjevik, *Phys. Fluids*, **13**, 1918 (1970).
5. S. P. Lin, *J. Fluid Mech*., **63**, 417 (1974).
6. H.-C. Chang, *Annu. Rev. Fluid Mech*., **26**, 103 (1994).
7. S. W. Joo, S. H. Davis and S. G. Bankoff, *J. Fluid Mech*., **230**, 117 (1991).
8. H. Kim, S. G. Bankoff and M. J. Miksis, *Phys. Fluids A*, **4**, 2117 (1992).
9. A. Pumir, P. Manneville and Y. Pomeau, *J. Fluid Mech*., **135**, 27 (1983).
10. Th. Prokopiou, M. Cheng and H.-C. Chang, *J. Fluid Mech*., **222**, 665 (1991).
11. H. Kim, S. G. Bankoff and M. J. Miksis, *J. Heat Trans. - T. ASME*, **116**, 986 (1994).
12. H. Kim, *Korean J. Chem. Eng*., **20**, 803 (2003).
13. E. Schäffer, T. Thurn-Albrecht, T. P. Russell and U. Steiner, *Nature*, **403**, 874 (2000).
14. E. Schäffer, T. Thurn-Albrecht, T. P. Russell and U. Steiner, *Europhys. Lett*., **53**, 518 (2001).
15. Z. Lin, T. Kerle, E. Schäffer, U. Steiner and T. P. Russell, *Macromolecules*, **35**, 3971 (2002).
16. H. Kim, *Korean J. Chem. Eng*., **14**, 41 (1997).
17. S. Wiggins, *Introduction to applied nonlinear dynamical systems and chaos*, Springer-Verlag, New York (1990).